Renormalization and scaling in quantum walks

Stefan Boettcher,[1] Stefan Falkner,[1] and Renato Portugal[2]
[1]*Department of Physics, Emory University, Atlanta, Georgia 30322, USA*
[2]*Laboratório Nacional de Computação Científica, Petrópolis, RJ 25651-075, Brazil*
(Received 14 January 2014; published 23 September 2014)

We show how to extract the scaling behavior of quantum walks using the renormalization group (RG). We introduce the method by efficiently reproducing well-known results on the one-dimensional lattice. For a nontrivial model, we apply this method to the dual Sierpinski gasket and obtain its exact, closed system of RG recursions. Numerical iteration suggests that under rescaling the system length, $L' = 2L$, characteristic times rescale as $t' = 2^{d_w} t$, with the exact walk exponent $d_w = \log_2 \sqrt{5} = 1.1609\ldots$. Despite the lack of translational invariance, this value is very close to the ballistic spreading, $d_w = 1$, found for regular lattices. However, we argue that an extended interpretation of the traditional RG formalism will be needed to obtain scaling exponents analytically. Direct simulations confirm our RG prediction for d_w and furthermore reveal an immensely rich phenomenology for the spreading of the quantum walk on the gasket. Invariably, quantum interference localizes the walk completely, with a site-access probability that decreases with a power law from the initial site, in contrast to a classical random walk, which would pass all sites with certainty.

DOI: 10.1103/PhysRevA.90.032324 PACS number(s): 03.67.Ac, 05.10.Cc, 05.40.Fb

I. INTRODUCTION

Following Grover's work [1], it was shown that discrete-time quantum walks [2–6] can access any chosen site of a regular lattice in two or more dimensions at least in $O(\sqrt{N \ln N})$ steps. Such a quadratic speedup over classical $O(N)$ first-passage times is one of the promising aspects of quantum computing, for instance, to search for items in an unsorted list. The fundamental importance of search algorithms to databases cannot be overstated, especially for hierarchical networks without translational invariance. For an example, we only need to mention Google's page-rank algorithm, for which a quantum version was recently proposed [7]. As fundamental as the random walk is to the description of classical diffusion and transport phenomena in physics [8,9] or the mixing times of randomized algorithms in computer sciences [10], the analogous quantum walk is rapidly rising in importance to describe a range of phenomena. Already, there are a number of experimental realizations of quantum walks, such as in waveguides [11,12], photonics [13,14], and optical lattices [15]. Therefore, classifying the *physical* behavior of quantum walks, their entanglement, localization, and interference effects in complex environments is interesting in its own right.

To date, only a very few analytical means [6,16] exist to describe the wealth of experimental and numerical observations. Aside from path-integral methods, these are mostly based on using a Fourier decomposition of the walk equation that presupposes a translational or relabeling symmetry between all sites. Accordingly, the general quantum walk on a simple line has now been relatively well explored [2–4], with a few forays into specific instances of two-dimensional lattices [5,17,18]. However, insistence on translational invariance leaves us with a limited understanding of the full impact of quantum interference effects, which are the origin of the quadratic speedup in the spreading on regular lattices. However, the range of studied systems remains too narrow to assess, let alone predict, how interference causes any particular scaling. In addition, localization effects emerge as soon as lattices possess loops [19–21] or disorder [22].

Here, we develop the venerable real-space renormalization group (RG) [23–25] to discover the long-range behavior of discrete-time quantum walks in more complex geometries. We introduce RG for the simple line, where we show how to reproduce the well-known ballistic spreading exponent, $d_w = 1$, by extending the traditional fixed point analysis into the complex plane [26]. For quantum walks on the dual Sierpinski gasket (DSG), iterating our exact recursions to $k = 21$ generations, which corresponds to a gasket with $N \approx 3^{21} \approx 10^{10}$ nodes, shows that time t rescales with baseline length L as $t \sim L^{d_w}$, with $d_w = 1.16096\ldots = \log_2 \sqrt{5}$, which is not quite ballistic but is spreading faster than a random walk on DSG [27], for which $d_w^{RW} = \log_2 5$. However, we find that localization effects diminish the magnitude of the wave function almost everywhere by $|\psi| \sim L^{-\beta}$, with $\beta = 0.424(3)$, such that *extensive* transport (which can still reach the boundaries for increasing L) decays with a power of L that is bounded between d_w and $d_w + 2\beta$, and we have $1 < d_w < d_w + 2\beta < d_w^{RW}$. We test our predictions with direct simulations on DSG with up to $k = 12$ generations.

This paper is organized as follows. In the next section, we introduce a formulation of the walk problem that allows us to study classical and quantum walks on comparable footing. In Sec. III, we apply the RG for walks, classical and quantum, on the simple line. In Sec. IV, we study the RG for the dual Sierpinski gasket. In Sec. V, we discuss the unusual aspects of the RG for quantum walks. In Sec. VI, we conclude with a summary of our results and outline future work.

II. FORMULATION OF THE WALK PROBLEM

The generic master equation for a discrete-time walk with a coin, whether classical or quantum, is

$$|\Psi(t+1)\rangle = \mathcal{U}|\Psi(t)\rangle, \tag{1}$$

where the time-evolution operator (or propagator) is written as

$$\mathcal{U} = \mathcal{S}(\mathcal{C} \otimes \mathcal{I}), \tag{2}$$

which contains the "shift" operator $\mathcal{S}$ and the coin $\mathcal{C}$. In the d-dimensional site basis $|\vec{n}\rangle$, we can describe the state of the system in terms of the site amplitudes $\psi_{\vec{n},t} = \langle \vec{n}|\Psi(t)\rangle$, which are simply the probability density to be at that site for a classical walk but represent a vector in coin space with each component having the amplitude for transitioning out of site $\vec{n}$ along one of its links for the quantum walk. Application of the coin $\mathcal{C}$ entangles these components, with subsequent redistribution of the walk to neighboring sites by the shift operator $\mathcal{S}$ based on those amplitudes. On the line, the shift operator for a homogeneous nearest-neighbor walk is

$$\mathcal{S} = \sum_x \{P \otimes |x-1\rangle\langle x| + Q \otimes |x+1\rangle\langle x| + R \otimes |x\rangle\langle x|\}, \tag{3}$$

with the shift matrices P and Q for moving left or right and R for staying in place, for instance,

$$P = \begin{pmatrix} 1 & 0 \\ 0 & 0 \end{pmatrix}, \quad Q = \begin{pmatrix} 0 & 0 \\ 0 & 1 \end{pmatrix}, \quad R = \begin{pmatrix} 0 & 0 \\ 0 & 0 \end{pmatrix}. \tag{4}$$

From Eq. (2), we get the propagator

$$\mathcal{U} = \sum_x \{A \otimes |x-1\rangle\langle x| + B \otimes |x+1\rangle\langle x| + M \otimes |x\rangle\langle x|\}, \tag{5}$$

with $A = P\mathcal{C}$, $B = Q\mathcal{C}$, and $M = R\mathcal{C}$, where the unitary coin matrix $\mathcal{C}$ is most generally given by [6]

$$\mathcal{C} = \begin{pmatrix} \sin\eta & e^{i\chi}\cos\eta \\ e^{i\vartheta}\cos\eta & -e^{i(\chi+\vartheta)}\sin\eta \end{pmatrix}. \tag{6}$$

In a quantum walk, the "hopping"operators A, B, and M are constrained by the requirement of unitary propagation, $\mathcal{I} = \mathcal{U}^\dagger\mathcal{U}$, which gives the conditions in coin space,

$$\mathcal{I}_d = A^\dagger A + B^\dagger B + M^\dagger M, \quad 0 = A^\dagger M + M^\dagger B = A^\dagger B, \tag{7}$$

implying that $A + B + M$ is unitary. As $\mathcal{C}$ is unitary, these conditions equally apply to P, Q, and R. They cannot be satisfied by scalars (except for trivial cases) [28,29].

The algebra in Eq. (7) requires at least two-dimensional matrices, and matching the dimension c of the coin space and the degree of each site represents a natural and commonly studied choice. For the d-dimensional hypercubic lattice, this means $c = 2d$, but higher-dimensional coins [20,21] and even coinless alternatives [28–32] have been studied.

III. RENORMALIZATION OF THE QUANTUM WALK ON A LINE

We introduce generating functions [9,33]

$$\tilde{\psi}_x(z) = \sum_{t=0}^{\infty} \psi_{x,t} z^t \tag{8}$$

to eliminate the explicit time dependence, which allows us to obtain the RG recursions. The asymptotic behavior for $t \to \infty$ is obtained in the limit of $z \to 1$, which puts more weight on terms with high values of t in Eq. (8). In the inverse transform of Eq. (8), the limit $z \to 1$ is intimately related to the large-time limit due to the crossover at $t(1-z) \sim 1$ in $z^t = \exp\{t \ln z\} \sim \exp\{-t(1-z)\}$ (see Ref. [9] or any textbook on generating functions).

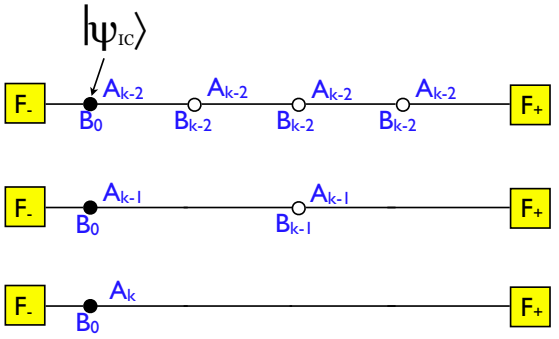

FIG. 1. (Color online) Absorption model for a simple line, indicating the three final recursion steps. Boxes represent absorbing sites, and sites indicated by black dots indicate the initial conditions $|\psi_{\rm IC}\rangle$. Labels A and B indicate the respective hopping parameters for each site.

The master equation (1) with $\mathcal{U}$ in Eq. (5) then becomes

$$\tilde{\psi}_x = zM\tilde{\psi}_x + zA\tilde{\psi}_{x-1} + zB\tilde{\psi}_{x+1} + \delta_{x,0}\psi_{\rm IC}. \tag{9}$$

For simplicity, we merely consider initial conditions (IC) localized at the origin, $\psi_{x,t=0} = \delta_{x,0}\psi_{\rm IC}$. As depicted in Fig. 1, we recursively eliminate $\tilde{\psi}_x$ for all sites for which x is an odd number and then set $x \to x/2$ and repeat each step for $k = 0,1,2,\ldots$. Each such step corresponds to a rescaling of the system size by a factor of 2; after k iterations, $\tilde{\psi}_x^{(k)}$ represents the renormalized wave function describing a domain of size 2^k, and the corresponding renormalized hopping parameters describe the effective transport in and out of that domain.

Therefore, starting at $k = 0$ with the "raw"hopping coefficients $A_0 = zA$, $B_0 = zB$, and $M_0 = zM$, after each step, the master equation becomes self-similar in form when redefining the renormalized hopping coefficients A_k, B_k, and M_k. For example, for consecutive sites near any even site x at step k we have [26]

$$\begin{aligned} \tilde{\psi}_{x-1} &= M_k\tilde{\psi}_{x-1} + A_k\tilde{\psi}_{x-2} + B_k\tilde{\psi}_x, \\ \tilde{\psi}_x &= M_k\tilde{\psi}_x + A_k\tilde{\psi}_{x-1} + B_k\tilde{\psi}_{x+1} + \delta_{x,0}\psi_{\rm IC}, \\ \tilde{\psi}_{x+1} &= M_k\tilde{\psi}_{x+1} + A_k\tilde{\psi}_x + B_k\tilde{\psi}_{x+2}. \end{aligned} \tag{10}$$

Solving for the central site x yields

$$\tilde{\psi}_x = M_{k+1}\tilde{\psi}_x + A_{k+1}\tilde{\psi}_{x-2} + B_{k+1}\tilde{\psi}_{x+2} + \delta_{x,0}\psi_{\rm IC}, \tag{11}$$

with RG "flow"

$$\begin{aligned} A_{k+1} &= A_k(I - M_k)^{-1}A_k, \\ B_{k+1} &= B_k(I - M_k)^{-1}B_k, \\ M_{k+1} &= M_k + A_k(I - M_k)^{-1}B_k + B_k(I - M_k)^{-1}A_k, \end{aligned} \tag{12}$$

where the hopping parameters, in general, are matrices.

A. Example: RG for the classical random walk

In the classical analysis [9,33] for a random walk with a Bernoulli coin p, Eqs. (12) reduce to

$$a_{k+1} = \frac{a_k^2}{1-m_k}, \quad b_{k+1} = \frac{b_k^2}{1-m_k}, \quad m_{k+1} = m_k + \frac{2a_kb_k}{1-m_k}, \tag{13}$$

with *scalar* quantities, which initiate at $k=0$ with $a_0 = zp$, $b_0 = z(1-p)$, and $m_0 = 0$. The fixed points (FPs) arising from this RG flow for $k \sim k+1 \to \infty$ at $z \to 1$ are $(a_\infty,b_\infty,m_\infty) = (0,0,m_\infty)$, $(1-m_\infty,0,m_\infty)$, or $(0,1-m_\infty,m_\infty)$ for any value of m^* on the unit interval [34].

Perturbing the RG flow in Eqs. (13) via $\{a,b,m\}_k \sim \{a,b,m\}_\infty + (1-z)\{\alpha,\beta,\mu\}_k$ for $z \to 1$ and large k, we find the linear system $(\alpha,\beta,\mu)_{k+1} = J \circ (\alpha,\beta,\mu)_k$ with the Jacobian

$$J = \left.\frac{\partial(a_{k+1},b_{k+1},m_{k+1})}{\partial(a_k,b_k,m_k)}\right|_{k\to\infty} = \begin{pmatrix} \frac{2a_\infty}{1-m_\infty}, & 0, & \frac{2b_\infty}{1-m_\infty} \\ 0, & \frac{2b_\infty}{1-m_\infty}, & \frac{2a_\infty}{1-m_\infty} \\ \frac{a_\infty^2}{(1-m_\infty)^2}, & \frac{b_\infty^2}{(1-m_\infty)^2}, & 1+\frac{2a_\infty b_\infty}{(1-m_\infty)^2} \end{pmatrix}. \quad (14)$$

The largest eigenvalue λ_w of this Jacobian, via $t(1-z) \sim 1$, then describes how time rescales, $t_k = \lambda_w t_{k-1}$, when the system length is doubled, $L_k = 2L_{k-1}$. Assuming a similarity solution for the probability density function of the walk, $\rho(x,t) \sim f(x^{d_w}/t)$, the scaling ansatz relating distance and time, $t_k \sim L_k^{d_w}$, thus provides

$$d_w = \log_2 \lambda_w. \quad (15)$$

Inserting the second and third FPs in J easily yields the ballistic solutions, $d_w = 1$, for drifting either to the left or to the right. In contrast, the undeterminedness of m_∞ in the first FP is peculiar. In fact, for $z=1$, $a_k + b_k + m_k = 1$ for all k, and starting from symmetric initial values $a_0 = b_0$, i.e., $p = \frac{1}{2}$, both remain identical and vanish together, $a_k \equiv b_k \to 0$, and $m_k \to m_\infty = 1$. Since both numerators and denominators in the Jacobian vanish, a correlated solution has to be constructed that "peals off" the leading behavior to glance into the boundary layer. Using $a_k \equiv b_k \sim a'_k \epsilon^k$ and $m_k \sim 1 - m'_k \epsilon^k$, assuming large k and $|\epsilon| < 1$, results in

$$a'_{k+1} = \frac{a'^2_k}{\epsilon m'_k}, \qquad m'_{k+1} = \frac{1}{\epsilon} m'_k - \frac{2a'^2_k}{\epsilon m'_k}, \quad (16)$$

with a single FP that self-consistently determines $\frac{a'_\infty}{m'_\infty} = \epsilon = \frac{1}{2}$. The Jacobian of these recursions, $J' = \frac{\partial(a'_{k+1},m'_{k+1})}{\partial(a'_k,m'_k)}|_{k\to\infty}$, at its FP gives $\lambda_w = 4$ as the largest eigenvalue; that is, $d_w = 2$ for the diffusive solution. In this formulation, even if we start with a vanishing self-term initially, $m_0 = 0$, the self-term ultimately dominates, $m_k \to 1$, reflecting the fact that in diffusion the renormalized domain of length $L_k \sim 2^k$ outgrows the walk such that almost all hops remain within that domain.

We note that the RG projects the salient properties of the walk into three "universality classes": diffusive and ballistic motion either to the left or right, characterized by an exponent $d_w = 2$ or 1. Each characterizes a fixed point of the dynamics, reached either for $p = \frac{1}{2}$ or $p \neq \frac{1}{2}$.

B. RG for the quantum walk on a line

For the quantum walk, we set

$$A_k = P_k \mathcal{C}, \qquad B_k = Q_k \mathcal{C}, \qquad M_k = R_k \mathcal{C}, \quad (17)$$

where, initially, $P_0 = zP$, $Q_0 = zQ$, and $R_0 = zR$ from Eq. (4). To gain insight, we evolve the RG flow (12) for a few iterations from these raw values. Each iteration consists of assembling the hopping parameters at level k according to Eq. (17), the actual RG step of applying Eqs. (12), and then the step of *inverting* Eq. (17) with $\mathcal{C}^{-1}$ to arrive at P_{k+1}, Q_{k+1}, and R_{k+1}. After two steps, a recurring pattern emerges that suggests the parametrization:

$$P_k = \begin{pmatrix} a_k & 0 \\ 0 & 0 \end{pmatrix}, \quad Q_k = \begin{pmatrix} 0 & 0 \\ 0 & -a_k \end{pmatrix}, \quad R_k = \begin{pmatrix} 0 & m_k \\ m_k & 0 \end{pmatrix}. \quad (18)$$

Indeed, for a_k and m_k, the RG flow (12) closes after each iteration with

$$a_{k+1} = \frac{a_k^2 \sin\eta}{1 - 2m_k \cos\eta + m_k^2}, \qquad m_{k+1} = m_k + \frac{(m_k - \cos\eta)a_k^2}{1 - 2m_k \cos\eta + m_k^2} \quad (19)$$

for $0 < \eta < \pi/2$ (setting $\chi = \vartheta = 0$). These recursions have a single fixed point at $(a_\infty,m_\infty) = (\sin\eta, \cos\eta)$, yet the Jacobian at $k \to \infty$ is η independent and has a degenerate eigenvalue $\lambda_w = 2$, suggesting $d_w = \log_2 \lambda = 1$. This reflects the well-known universality of the large-scale dynamics of the quantum walk on the line with respect to the chosen coin [4].

As we will show in Sec. V, however, this picture may be incomplete, a lucky accident due to the fact that the "fractal" exponent $d_f = \log_2 \lambda_f = 1$ and the walk exponent d_w coincide. To exemplify this aspect here, let us consider the probability F_a of *ever* being absorbed at a site $x = a$ as a simple and generic observable [4,35]. From Eq. (8), for a random walk with $\rho(x,t) = \psi_{x,t}$, it is simply $F_a = \sum_t \psi_{a,t} = \lim_{z\to 1} \tilde{\psi}_a(z)$. For a quantum walk, it is instead $\rho(x,t) = |\psi_{x,t}|^2$, and hence,

$$F_a = \sum_{t=0}^{\infty} |\psi_{a,t}|^2 = \oint \frac{dz}{2\pi i z} |\tilde{\psi}_a(z)|^2 = \int_{-\pi}^{\pi} \frac{d\theta}{2\pi} |\tilde{\psi}_a(\theta)|^2, \quad (20)$$

where we choose

$$z = -e^{i\theta} \qquad (-\pi < \theta \leqslant \pi), \quad (21)$$

i.e., $z \to -1$ for $\theta \to 0$ as a reference point (see below). While the random walk merely entails a local analysis for real $z \to 1$ [9], the unitarity of quantum walks generally demands an analysis along the *entire* unit circle in the complex-z plane. Let us put the quantum walk on the line between two absorbing walls $F_\pm$, as shown in Fig. 1, with $F_-^{(k)}$ at $x_- = -1$ right next to the starting site $x = 0$; the wall $F_+^{(k)}$ at site $x_+ = 2^k$ recedes farther away from the starting site with every iteration of the flow equations. In Fig. 2(a), we plot the integrand $|\tilde{\psi}_+^{(k)}(z)|$ for $\arg z = \pi - \theta$ on the unit circle. Some algebra shows that $\tilde{\psi}_+^{(k)}(z) \propto a_k$, which depends on z through a_0. The asymptotic behavior of a_k in Eq. (19) for large k at fixed θ falls into one of four different cases: (i) At $\theta = 0$ and $\theta = \pi$, the stationary behavior for the aforementioned fixed point is obtained. (ii) For $0 < |\theta| < \eta$ and $0 < \pi - |\theta| < \eta$, a_k varies *chaotically* with k. (iii) For $|\theta| = \eta$ and $|\theta| = \pi - \eta$ local analysis recovers classical diffusive scaling. (iv) For $\eta < |\theta| < \pi - \eta$, a_k vanishes exponentially with $N = 2^k$. We argue that only the chaotic regimes, $|\theta| < \eta$ and $\pi - |\theta| < \eta$, with

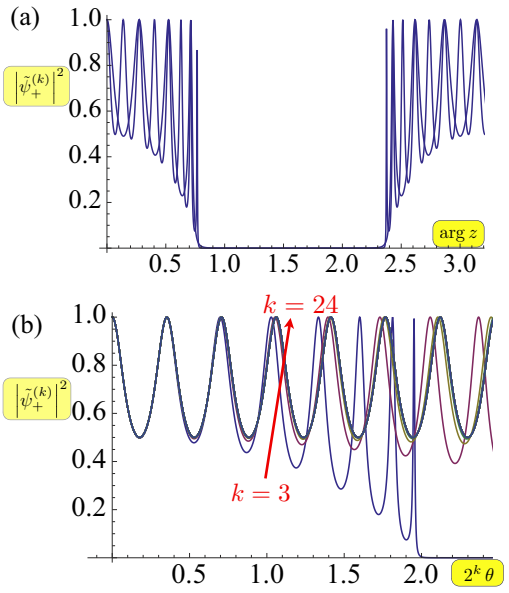

FIG. 2. (Color online) Plot of $|\tilde{\psi}_+^{(k)}(z)|$ at $\eta = \pi/4$ and generic initial conditions $\psi_{\rm IC} = (0,1)$ (a) for $\arg z$ after $k = 2,3$ iterations and (b) for the rescaled variable $2^k\theta$, $z = -e^{i\theta}$, to collapse all data up to $k = 24$ for $\theta \to 0$. As (a) shows, the integrand is periodic with period π and has significant support only for $|\theta| < \eta$ and $\pi - |\theta| < \eta$.

the stationary points at their centers contribute to extensive quantum transport [36]. That is, it can be shown that for $\eta \to 0$ the "velocity" of the ballistically spreading quantum walk decreases to zero and eventually becomes localized for $\eta = 0$, exactly when both chaotic regimes shrink to zero, while the stationary point remains inside.

Clearly, quantum transport here is determined by properties of the entire wave function $\tilde{\psi}_x(z)$, not just the limit $z \to z_0$ near some fixed point z_0. We will analyze this situation in more detail in Sec. V.

IV. RENORMALIZATION OF THE QUANTUM WALK ON THE DUAL SIERPINSKI GASKET

The DSG is a degree-3 lattice (see Fig. 3), and unitarity requires at least a $(c = 3)$-dimensional coin. As the most general such coin has six real parameters, we focus here on only the real and symmetric Grover coin,

$$\mathcal{C} = \frac{1}{3}\begin{pmatrix} -1 & 2 & 2 \\ 2 & -1 & 2 \\ 2 & 2 & -1 \end{pmatrix}, \tag{22}$$

and we defer generalizations to future discussions. Note that DSG has several advantages over the more familiar Sierpinski gasket. DSG is a regular degree-3 lattice, while the Sierpinski gasket itself is a regular degree-4 lattice. However, it is not merely the higher degree that causes difficulties for quantum walks on the original Sierpinski gasket. The internal coin degrees of freedom cause a labeling problem that severely complicates its consideration, as shown in Ref. [37]. Interestingly, none of these problems exist for the classical random walk, and the Sierpinski gasket (or its dual counterpart) serves as a popular example of a simple demonstration of

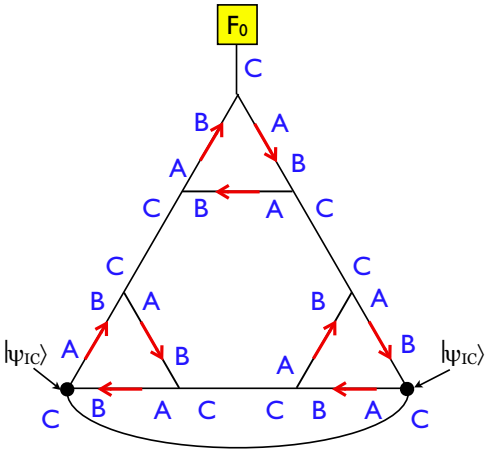

FIG. 3. (Color online) Absorption model for the dual Sierpinski gasket at generation $k = 1$. The box represents the absorbing site, and sites marked by black dots indicate the initial conditions $|\psi_{\rm IC}\rangle$. Labels A,B,C indicate the respective hopping parameters for leaving each site. Note that for increasing generation k, the minimal separation between initiating sites and the sole absorbing site will increase as $\sim 2^k$.

the RG because its hierarchical structure and high degree of symmetry affect a RG flow in a *single* real hopping parameter. For the quantum walk, we will find instead *five* coupled complex recursions with a large number of terms.

A. Renormalization of the dual Sierpinski gasket

Figure 3 shows the elementary graphlet of nine sites that is used to construct the DSG. It also represents the basic unit from which we can extract the flow equations by tracing out the wave functions $\tilde{\psi}_4,\ldots,\tilde{\psi}_9$ on the six inner sites, leaving only the three corner sites $\tilde{\psi}_1,\ldots,\tilde{\psi}_3$ and the renormalized hopping coefficients between them. Note the systematic labeling for each of the three outbound directions at every site that determines, in effect, which shift operator applies to that direction. The master equations relating those nine sites are

$$\begin{aligned}
\tilde{\psi}_1 &= M_k\tilde{\psi}_1 + C_k\tilde{\psi}_{\bar{1}} + A_k\tilde{\psi}_4 + B_k\tilde{\psi}_5,\\
\tilde{\psi}_2 &= M_k\tilde{\psi}_2 + C_k\tilde{\psi}_{\bar{2}} + A_k\tilde{\psi}_6 + B_k\tilde{\psi}_7,\\
\tilde{\psi}_3 &= M_k\tilde{\psi}_3 + C_k\tilde{\psi}_{\bar{3}} + A_k\tilde{\psi}_8 + B_k\tilde{\psi}_9,\\
\tilde{\psi}_4 &= M_k\tilde{\psi}_4 + C_k\tilde{\psi}_9 + A_k\tilde{\psi}_5 + B_k\tilde{\psi}_1,\\
\tilde{\psi}_5 &= M_k\tilde{\psi}_5 + C_k\tilde{\psi}_6 + A_k\tilde{\psi}_1 + B_k\tilde{\psi}_4,\\
\tilde{\psi}_6 &= M_k\tilde{\psi}_6 + C_k\tilde{\psi}_5 + A_k\tilde{\psi}_7 + B_k\tilde{\psi}_2,\\
\tilde{\psi}_7 &= M_k\tilde{\psi}_7 + C_k\tilde{\psi}_8 + A_k\tilde{\psi}_2 + B_k\tilde{\psi}_6,\\
\tilde{\psi}_8 &= M_k\tilde{\psi}_8 + C_k\tilde{\psi}_7 + A_k\tilde{\psi}_9 + B_k\tilde{\psi}_3,\\
\tilde{\psi}_9 &= M_k\tilde{\psi}_9 + C_k\tilde{\psi}_4 + A_k\tilde{\psi}_3 + B_k\tilde{\psi}_8.
\end{aligned} \tag{23}$$

Here, $\tilde{\psi}_{\bar{1}},\ldots,\tilde{\psi}_{\bar{3}}$ refer to the corner sites of the respective neighboring graphlets, which do not get renormalized themselves.

The algebraic effort is drastically reduced by tracing out $\tilde{\psi}_4,\ldots,\tilde{\psi}_9$ in a symmetrical way. When eliminated, each of those amplitudes must be a function of the remaining three,

$\tilde{\psi}_1,\ldots,\tilde{\psi}_3$, in a cyclically permuted manner. Thus, we start with the ansatz

$$\tilde{\psi}_4 = a\tilde{\psi}_1 + b\tilde{\psi}_2 + c\tilde{\psi}_3, \quad \tilde{\psi}_5 = d\tilde{\psi}_1 + e\tilde{\psi}_2 + f\tilde{\psi}_3, \quad (24)$$

and we proceed similarly for the inner sites at the other two corners, $(\tilde{\psi}_6,\tilde{\psi}_7)$ and $(\tilde{\psi}_8,\tilde{\psi}_9)$, by appropriately permuting the indices on $\tilde{\psi}_1,\ldots,\tilde{\psi}_3$. Inserting these prospective solutions into the right-hand side of the last six relations in Eqs. (23) and comparing coefficients with Eqs. (24) provide self-consistency relations for the matrices $a,\ldots,f$. This step eliminates $\tilde{\psi}_4,\ldots,\tilde{\psi}_9$ by transforming the problem into one of expressing matrices $a,\ldots,f$ in terms of A_k,B_k,C_k, and M_k, or, with simpler notation, $\bar{A} = (I - M_k)^{-1}A_k$, $\bar{B} = (I - M_k)^{-1}B_k$, and $\bar{C} = (I - M_k)^{-1}C_k$. Most important, this ansatz has disentangled the original six equations into two *equivalent, closed* sets of three relations that can be solved independently: Since comparing coefficients provides a bipartite set of relations initially,

$$\begin{aligned} a &= \bar{A}d + \bar{C}e + \bar{B}, & d &= \bar{B}a + \bar{C}c + \bar{A}, \\ b &= \bar{A}e + \bar{C}f, & e &= \bar{B}b + \bar{C}a, \\ c &= \bar{A}f + \bar{C}d, & f &= \bar{B}c + \bar{C}b \end{aligned} \quad (25)$$

(note that these are noncommuting matrices), we write

$$\begin{aligned} a &= \bar{A}\bar{B}a + \bar{A}\bar{C}c + \bar{A}^2 + \bar{C}\bar{B}b + \bar{C}^2a + \bar{B}, \\ b &= \bar{A}\bar{B}b + \bar{A}\bar{C}a + \bar{C}\bar{B}c + \bar{C}^2b, \\ c &= \bar{A}\bar{B}c + \bar{A}\bar{C}b + \bar{C}\bar{B}a + \bar{C}^2c + \bar{C}\bar{A}, \end{aligned} \quad (26)$$

and we write a corresponding set for d,e,f by identifying $a \Leftrightarrow d, b \Leftrightarrow f, c \Leftrightarrow e$, and $\bar{A} \Leftrightarrow \bar{B}$, while $\bar{C}$ remains in place. To minimize the number of matrix multiplications, it is now convenient to abbreviate

$$\begin{aligned} V &= \left(I - \bar{A}\bar{B} - \bar{C}^2\right)^{-1}, \\ \mathcal{A} &= V\bar{A}\bar{C}, \\ \mathcal{B} &= V\bar{C}\bar{B}, \\ W &= (I - \mathcal{B}\mathcal{A})^{-1}, \\ X &= \mathcal{A}^2 + \mathcal{B}, \\ Y &= W(\mathcal{A} + \mathcal{B}^2), \\ Z &= WV(A^2 + B). \end{aligned} \quad (27)$$

With these abbreviations, we find

$$\begin{aligned} c &= [I - \mathcal{A}\mathcal{B} - XY]^{-1}\left(V\bar{C}\bar{A} + XZ\right), \\ a &= Yc + Z, \\ b &= \mathcal{A}a + \mathcal{B}c, \end{aligned} \quad (28)$$

and the complementing set for d,e, and f. Finally, inserting $\tilde{\psi}_4,\tilde{\psi}_5$ from Eqs. (24) into the relation for $\tilde{\psi}_1$ (or, equivalently, inserting $\tilde{\psi}_6,\tilde{\psi}_7$ into the relation for $\tilde{\psi}_2$ or $\tilde{\psi}_8,\tilde{\psi}_9$ into that for $\tilde{\psi}_3$) yields the renormalization flow

$$\begin{aligned} M_{k+1} &= M_k + A_k a + B_k d, \quad A_{k+1} = A_k c + B_k f, \\ B_{k+1} &= A_k b + B_k e, \quad C_{k+1} = C_k. \end{aligned} \quad (29)$$

(Note that C_k does not renormalize.) While tedious to derive, these equations are exact and easily implemented on a computer algebra system.

B. Parametrizing the RG flow for the dual Sierpinski gasket

As in Sec. III B, we define shift matrices

$$P = \begin{bmatrix} 1 & 0 & 0 \\ 0 & 0 & 0 \\ 0 & 0 & 0 \end{bmatrix}, \quad Q = \begin{bmatrix} 0 & 0 & 0 \\ 0 & 1 & 0 \\ 0 & 0 & 0 \end{bmatrix}, \quad R = 0. \quad (30)$$

Since C_k does not renormalize, $C_k = C_0$, it does not require a parametrization. We initiate the recursions at $k = 0$ with $A_0 = zPC, B_0 = zQC$, and $M_0 = zRC = 0$. After a single iteration, a recursive pattern emerges that suggests a five-parameter ansatz:

$$\begin{aligned} P_k &= \begin{pmatrix} a_k^{(1)} & a_k^{(2)} & 0 \\ a_k^{(2)} & a_k^{(3)} & 0 \\ 0 & 0 & 0 \end{pmatrix}, \quad Q_k = \begin{pmatrix} a_k^{(3)} & a_k^{(2)} & 0 \\ a_k^{(2)} & a_k^{(1)} & 0 \\ 0 & 0 & 0 \end{pmatrix}, \\ R_k &= \frac{1}{2}\begin{pmatrix} m_k^{(1)} - m_k^{(2)} & m_k^{(1)} + m_k^{(2)} & 0 \\ m_k^{(1)} + m_k^{(2)} & m_k^{(1)} - m_k^{(2)} & 0 \\ 0 & 0 & 0 \end{pmatrix}. \end{aligned} \quad (31)$$

Iteration provides of *closed* set of five complex recursions, $\{a_{k+1}^{(1,2,3)},m_{k+1}^{(1,2)}\} = \mathcal{R}(\{a_k^{(1,2,3)},m_k^{(1,2)}\};z)$, each a ratio of polynomials similar to Eqs. (19) but with *dozens* of terms and an explicit dependence on z due to C_0. Again, the algebra is easily handled by a computer; however, these recursions prove numerically unstable, and numerical precision is quickly lost near points of interest, such as $z = -1$.

C. Asymptotic properties of the RG flow

As a specific observable to study, we again focus on the probability to ever get absorbed at a wall, as shown in Fig. 3. With increasing length L, the sole absorbing site at one corner of DSG recedes from the starting point of the quantum walk (IC), chosen at the opposite corner. Thus, the total absorption $F_0^{(k)}$ is a measure of quantum transport across the system. Figure 4(a) shows the integrand $|\tilde{\psi}_0^{(k)}(z)|^2$ of F_0 in Eq. (20) for $0 \leqslant \arg z \leqslant \pi$ (all observables are symmetric around the real-z axis). We derive the expression for $\tilde{\psi}_0$ in Eq. (A7) in the Appendix. Compared to Fig. 2(a) for the line, remarkably complex patterns emerge for a quantum walk on DSG:

(1) There is an *isolated* stationary point at $\arg z = \pi$, i.e., $\theta = 0$ [see Eq. (21)], where $a_k^{(1,2,3)} = -m_k^{(1)} = -\frac{1}{3}$ and $m_k^{(2)} = 1$ for all $k \geqslant 2$.

(2) A sequence of sparse, rugged peaks that slowly decay seem to accumulate for $\theta \to 0$ with increasing k.

(3) Everywhere else, the function decays rapidly for increasing k, where $a_k^{(1)} \sim a_k^{(2)} \sim a_k^{(3)} \to 0$ and $|m_k^{(1,2)}| \to 1$. There is *no* finite oscillatory domain to signal extensive quantum transport. Instead, since $\tilde{\psi}_0^{(k)} \sim a_k^{(1,2,3)}$, it is easy to show from the five recursions that for any *fixed* value of $\theta \neq 0$, $|\tilde{\psi}_0^{(k)}(z)| \to 0$ for $k \to \infty$, suggesting that for large systems quantum transport ceases such that the absorption approaches zero.

Unlike for translation-invariant lattices, where some fraction of quantum walks might localize, on DSG the *entire* walk eventually gets trapped. However, unlike the sharp localization on lattices [20,21], the entrapped portion of the wave function has broad tails here. Only at $\theta = 0$ do we find a fixed point. The largest eigenvalue of its Jacobian is $\lambda_f = 3$, which coincides with the fractal exponent of DSG, $d_f = \log_2 3$. However, the

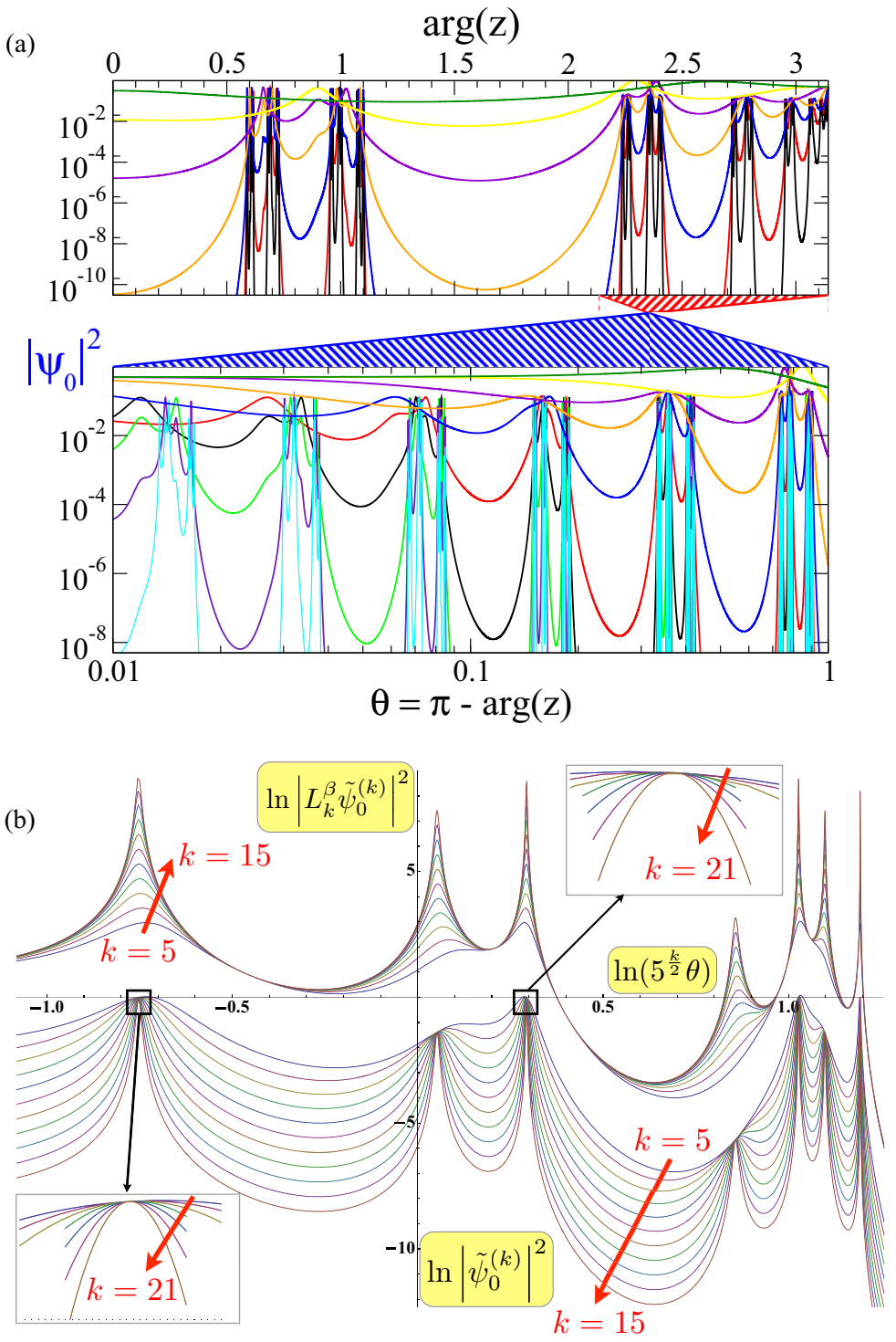

FIG. 4. (Color online) (a) Log plot of the integrand $|\tilde{\psi}_0^{(k)}(z)|$ in Eq. (20) for $0 \leqslant \arg z \leqslant \pi$ for $k = 1, \ldots 6$. Decaying almost everywhere, the integrand has the most support near the fixed point, $\arg z \to \pi$. A logarithmic scale with $\theta = \pi - \arg z \to 0$ reveals a self-similar sequence of periodic structures. (b) Scaling collapse of $|L_k^\beta \tilde{\psi}_0^{(k)}(z)|$ with $L_k = 2^k$ for $\ln(\lambda_w^k \theta)$ at $k = 5, \ldots, 15$ using $\lambda_w = \sqrt{5}$. At $\beta = 0$, all data line up; in particular, all peaks remain constant (= 1 up to $k = 21$; see the insets) but narrow. At $\beta = 0.424(3)$, all data in the fast-decaying intervals collapse, but the peaks now diverge.

data collapse in Fig. 4(b) demonstrates that the limit $\theta \to 0$ is singular: all data align and collapse according to Eq. (32) but with an eigenvalue *smaller* than the Jacobian. This collapse occurs in a regime such that $\lambda_w^k \theta \sim 1$, while the fixed point at $\ln \theta \to -\infty$ seems infinitely far away and irrelevant. We will discuss this point in more detail in Sec. V.

The exponents λ_w and β from Eq. (32) can be determined recursively with high accuracy from the collapse with

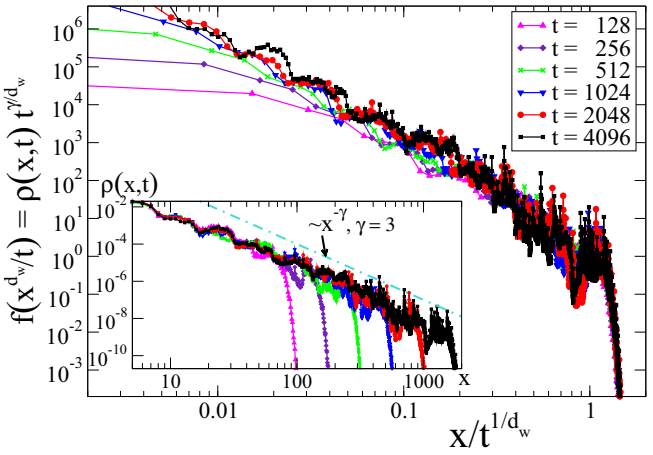

FIG. 5. (Color online) Simulations of quantum walks on DSG for the collapse $f(x^{d_w}/t) \sim \rho(x,t)t^{\gamma/d_w}$, with $d_w = \log_2 \sqrt{5}$, for the probability density function $\rho(x,t) = |\psi_{x,t}|^2$ (see inset) for finding the walker at any site x hops away from the initial sites at times $t = 2^l$, $l = 7,\ldots,12$, on a DSG of size $N \sim 3^{12}$, before the absorbing wall is reached. To fit not only the cutoff but also the bulk distribution, we estimate a power-law decay with exponent $\gamma \approx 3$ for ρ as a function of x; see the inset.

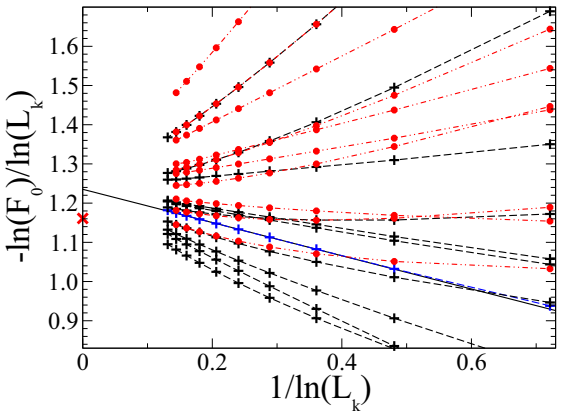

FIG. 6. (Color online) Extrapolation for the scaling exponent in the decay of the simulated absorption F_0 with system length $L_k = 2^k$, $k \leqslant 12$, based on a power law, for many different symmetric (pluses) and asymmetric (dots) initial conditions (IC). All data appear to extrapolate to the same intercept ($L_k \to \infty$) at about 1.23(1), with the most linear fit (extended line) provided by the symmetric $\psi_{\rm IC} \propto (1,2,1)$. This exponent is closely bounded below by $d_w = \log_2 \sqrt{5}$ (cross).

computational cost linear in k (i.e., logarithmic in system size). As shown at the bottom of Fig. 4(b) and especially in the insets, lining up the data for $|\tilde{\psi}_0^{(k)}(z)|$, $k = 5,\ldots,21$, without resizing ($\beta = 0$) yields $\lambda_w = 2.23607(2)$, which we identify as $\lambda_w = \sqrt{5}$, such that $d_w = \log_2 \lambda_w = \log_2 \sqrt{5}$. (The only limitation in the ability to determine the value of λ_w to arbitrary accuracy numerically is set by the chaotic nature of the RG recursions; initiating z near $\theta \to 0$ with 1500-digit accuracy, no accuracy remains after only $k = 25$ iterations.)

To demonstrate the relevance of this eigenvalue λ_w for the asymptotic spreading of the quantum walk, we have directly conducted large-scale numerical simulations of the master equation (see Fig. 5). The value of $d_w = \log_2 \sqrt{5}$ causes a data collapse for $\rho(x,t) \sim f(x^{d_w}/t)/t^{\gamma/d_w}$, with $\gamma \approx 3$, from fitting $\rho(x,t) \sim x^{-\gamma}$ (see the inset in Fig. 5). (The origin of this power-law decay, in contrast to a Gaussian kernel for diffusion, is as yet unknown.) In particular, the inset shows that the cutoff in $\rho(x,t)$ scales perfectly as $x_{\rm co} \sim t^{1/d_w}$, leading to the collapse in the main panel.

However, this shift in θ alone results in a set of functions that *uniformly decay* with increasing k everywhere but in isolated points [see the down arrows in Fig. 4(b)]. Using $\beta = 0.424(3)$ in Eq. (32) collapses the data everywhere except for isolated peaks that now *grow* with k [see the up arrows in Fig. 4(b)]. The absorption integral from Eq. (20) that receives most of its support near $|\theta| < \epsilon \ll 1$ yields $F_0^{(k)} \sim F_0^{(k-1)}/(\lambda_w 2^{2\beta})$, using Eq. (32), with the solution $F_0^{(k)} \sim L_k^{-(d_w+2\beta)}$, $L_k \sim 2^k$, as a lower bound on the adsorption. Thus, the true $F_0^{(k)}$ vanishes with length L as a power law with an exponent *at least* as large as d_w ($\beta = 0$) but not larger than $d_w + 2\beta \approx 2.01(1)$. Simulations of quantum walks on DSG up to $k = 12$ generations shown in Fig. 6 suggest a *unique* exponent $\approx$1.23(1) that is only minutely above d_w, independent of the IC.

V. HOW RG FIXED POINTS FAIL TO DETERMINE ASYMPTOTIC PROPERTIES

As Sec. IV A has shown, extracting the scaling $\rho(x,t) \sim f(x^{d_w}/t)$ from the fixed point proves *insufficient* for the quantum walk on DSG. While the fixed point of the RG for the quantum walk on the line naively appears to reproduce the known scaling properties, the discussion shows that this is likely a coincidence for this rather simple scenario. The examples of the line in Sec. III and of DSG in Sec. IV show the fixed point found in both cases appear to coincide with the fractal exponent $d_f = \log_2 \lambda_f$, which refers to structural properties of the lattice, rather than to the dynamics of the walk itself.

Since most dynamic observables require an extended examination in the complex-z plane, the example of the Sierpinski gasket suggests that the same holds true for the RG flow. As the data collapse in Fig. 4 demonstrates, the way to extract the eigenvalue λ_w (and hence d_w) that is consistent with the RG on fractals (such as DSG below) results from the scaling

$$\tilde{\psi}_a^{(k)}(\theta) \sim 2^{-\beta} \tilde{\psi}_a^{(k-1)}(\lambda_w \theta) \tag{32}$$

at large k near a fixed point for $\theta \to 0$, such that $\lambda_w^k \theta \gtrsim 1$. Rescaling θ corresponds to $z \to z^{1/\lambda_w}$ for $k \to k+1$, and hence, from Eq. (8) we see that it amounts to a rescaling of time t with λ_w when L doubles, such that $d_w = \log_2 \lambda_w$. The scenario posed by Eq. (32) is depicted in Fig. 7, which suggests that the RG flow will have to be solved asymptotically in an intermediate scaling regime, as it can never reach the fixed point for $\lambda_w < \lambda_f$. While such an exact analysis has not been achieved yet, the simplicity of the exponent suggests that it should be achievable. It suggests that the RG for quantum walks requires an entirely new approach, beyond the usual fixed-point analysis.

The fixed-point analysis happened to be successful for the *1d* line because fractal and walk exponents coincide there,

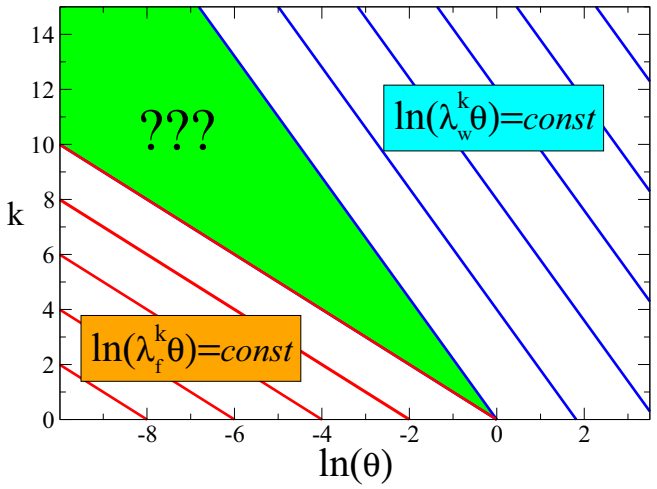

FIG. 7. (Color online) Depiction of the characteristic trajectories along which the RG flow remains invariant, where $\theta = \arg(z - z_0)$ is a measure of the angular distance from the fixed point at z_0 in the complex unit circle. In this picture, the fixed point is off to the left at $\ln\theta = -\infty$, where the data collapse by way of the fractal exponent $d_f = \log_2 \lambda_f$ [red (light gray) trajectories], resulting from the largest Jacobian eigenvalue λ_f. On the right, where $\lambda_w^k \theta \gtrsim 1$ [blue (dark gray) trajectories], a far more subtle collapse like that shown in Fig. 4 results. Note that those trajectories cannot ever reach the fixed point since $\lambda_w < \lambda_f$ and will require some intermediate scaling ansatz (except for the quantum walk on a line, where $\lambda_f = \lambda_w$). The green (gray) shaded area between those different characteristics marks an unknown crossover region.

$d_w = d_f = d = 1$ (and $\beta = 0$ there), as demonstrated by the data collapse in Fig. 2(b). As the limit $\theta \to 0$ for the simple line is not singular, it is not surprising that scaling collapse and traditional RG analysis near the fixed point provide identical results.

VI. CONCLUSIONS

In conclusion, we have devised a method to determine the asymptotic behavior of discrete-time quantum walks on the dual Sierpinski gasket using RG. Fractal graphs, as well as random networks, lack the translational symmetry that is essential to study quantum walks on lattices. The present treatment can be applied to renormalizable structures [9] to generate analytical results for important physical quantities such as the spreading rate of the probability distributions. However, compared to random walks, quantum walks require extending RG into the complex plane, which we have explored in some detail. We confirmed that quantum walks are more intricate than random walks, and we analyzed the effects of geometry on quantum interference. Direct numerical simulations support our conclusions.

The RG analysis for quantum walks appears to be more complicated than for classical random walks, likely a result of unitarity, which precludes the typical contractive mapping that makes RG of classical, stochastic processes easy. However, our results suggest that such quantum systems will ultimately find just as exact a description as those for classical systems. In turn, much more will be gained, as these quantum processes exhibit a far richer phenomenology compared to the rather structureless diffusion process.

Finally, we note that the potential scope of the RG is much broader [24] than being merely a toll to calculate exponents for some specific fractals, where it happens to be exact. Once the present technical issues have been resolved, it should be possible to use the RG, exactly or approximately, to classify the asymptotic properties of quantum walks and, hopefully, other quantum algorithms into universality classes. Such a classification ultimately should serve as the basis for understanding and hence controlling the observed behaviors.

ACKNOWLEDGMENTS

We acknowledge financial support from CNPq, LNCC, and the US National Science Foundation through Grant No. DMR-1207431. S.B. thanks LNCC for its hospitality and acknowledges financial support from a research fellowship from the "Ciencia sem Fronteiras" program in Brazil.

APPENDIX

1. Absorption on the line

We consider the case of two absorbing walls on both ends of a simple line with the initial conditions (IC) located on a single site right next to the left wall, as shown in Fig. 1. It is convenient to identify the IC site as the origin ($i = 0$); that is, the left-absorbing site is $\tilde{\psi}_-$, and the right wall is located on site $i = 2^k$ with $\tilde{\psi}_+$. Since nothing escapes out of the absorbing sites, we have the following master equations:

$$\begin{aligned}
\tilde{\psi}_- &= B_0\tilde{\psi}_0,\\
\tilde{\psi}_0 &= N_0\tilde{\psi}_0 + B_0\tilde{\psi}_1 + \psi_{\mathrm{IC}},\\
\tilde{\psi}_x &= M_0\tilde{\psi}_x + A_0\tilde{\psi}_{x-1} + B_0\tilde{\psi}_{x+1} \quad (1 \leqslant i \leqslant 2^k - 2),\\
\tilde{\psi}_{2^k-1} &= M_0\tilde{\psi}_{2^k-1} + A_0\tilde{\psi}_{2^k-2},\\
\tilde{\psi}_+ &= A_0\tilde{\psi}_{2^k-1}.
\end{aligned} \tag{A1}$$

This setup has been chosen exactly such that *all* quantities renormalize according to the flow in (12), avoiding some of the special considerations typically required near boundaries. The only exception refers to the self-term at $\tilde{\psi}_0$: Although initially $N_0 = M_0 = 0$, its recursion is $N_{k+1} = N_k + B_k(I - M_k)^{-1}A_k$ instead. (This geometry resembles exactly the setup of Ref. [35], with which we can now compare.)

In each recursion step, every second intervening site still present is eliminated (see the sequence in Fig. 1). As the last setting suggests, we are left with three relations,

$$\tilde{\psi}_- = B_0\tilde{\psi}_0, \quad \tilde{\psi}_0 = N_k\tilde{\psi}_0 + \psi_{\mathrm{IC}}, \quad \tilde{\psi}_+ = A_k\tilde{\psi}_0. \tag{A2}$$

We now simply eliminate $\tilde{\psi}_0$ to get

$$\tilde{\psi}_-^{(k)} = B_0(1 - N_k)^{-1}\psi_{\mathrm{IC}}, \quad \tilde{\psi}_+^{(k)} = A_k(1 - N_k)^{-1}\psi_{\mathrm{IC}}. \tag{A3}$$

2. Absorption on the dual Sierpinski gasket

Using the recursions developed in Eqs. (29), we exactly evolve from the raw hopping coefficients A_0, B_0, and M_0 (C

does not renormalize, i.e., $C_k = C_0$) to the kth stage; the next to last stage is shown in Fig. 3. After tracing out the remaining six inner sites, we have

$$\begin{aligned}
\tilde{\psi}_0 &= C_0\tilde{\psi}_1,\\
\tilde{\psi}_1 &= M_k\tilde{\psi}_1 + A_k\tilde{\psi}_3 + B_k\tilde{\psi}_2,\\
\tilde{\psi}_2 &= M_k\tilde{\psi}_2 + A_k\tilde{\psi}_1 + (B_k + C_0)\tilde{\psi}_3 + \frac{1}{\sqrt{2}}\psi_{\mathrm{IC}},\\
\tilde{\psi}_3 &= M_k\tilde{\psi}_3 + (A_k + C_0)\tilde{\psi}_2 + B_k\tilde{\psi}_1 + \frac{1}{\sqrt{2}}\psi_{\mathrm{IC}}.
\end{aligned} \tag{A4}$$

Here, we assume symmetric IC applied at the two corner sites opposite the absorbing wall; the procedure is easily extended to two unequal IC. For $\eta \in \{A_k, B_k, C_0, \psi_{\mathrm{IC}}\}$ we define $\bar{\eta}_k = (I - M_k)^{-1}\eta_k$ and make the ansatz

$$\tilde{\psi}_2 = X\tilde{\psi}_1 + U\bar{\psi}_{\mathrm{IC}}, \quad \tilde{\psi}_3 = Y\tilde{\psi}_1 + V\bar{\psi}_{\mathrm{IC}}. \tag{A5}$$

Inserting $\tilde{\psi}_{2,3}$ into Eqs. (A4) determines self-consistently

$$\begin{aligned}
X &= [I - (\bar{A}_k + \bar{C}_0)(\bar{B}_k + \bar{C}_0)]^{-1}[\bar{B}_k + (\bar{A}_k + \bar{C}_0)\bar{A}_k],\\
Y &= [I - (\bar{B}_k + \bar{C}_0)(\bar{A}_k + \bar{C}_0)]^{-1}[\bar{A}_k + (\bar{B}_k + \bar{C}_0)\bar{B}_k],\\
U &= [I - (\bar{A}_k + \bar{C}_0)(\bar{B}_k + \bar{C}_0)]^{-1}[I + (\bar{A}_k + \bar{C}_0)],\\
V &= [I - (\bar{B}_k + \bar{C}_0)(\bar{A}_k + \bar{C}_0)]^{-1}[I + (\bar{B}_k + \bar{C}_0)].
\end{aligned} \tag{A6}$$

Inserting $\tilde{\psi}_{2,3}$ in Eqs. (A5) into $\tilde{\psi}_1$ in Eqs. (A4), and then $\tilde{\psi}_1$ into $\tilde{\psi}_0$, yields

$$\tilde{\psi}_0 = C_0(I - \bar{A}_k X - \bar{B}_k Y)^{-1}(\bar{A}_k U + \bar{B}_k V)\bar{\psi}_{\mathrm{IC}}. \tag{A7}$$

[1] L. K. Grover, Phys. Rev. Lett. **79**, 325 (1997).
[2] D. Aharonov, A. Ambainis, J. Kempe, and U. Vazirani, in *Proceedings of the 33rd Annual ACM Symposium on Theory of Computing (STOC 2001)* (Association for Computing Machinery, New York, 2001), pp. 50–59.
[3] N. Shenvi, J. Kempe, and K. B. Whaley, Phys. Rev. A **67**, 052307 (2003).
[4] E. Bach, S. Coppersmith, M. P. Goldschen, R. Joynt, and J. Watrous, J. Comput. Syst. Sci. **69**, 562 (2004).
[5] A. Ambainis, J. Kempe, and A. Rivosh, in *Proceedings of the 16th Annual ACM-SIAM Symposium on Discrete Algorithms (SODA 2005)* (Society for Industrial and Applied Mathematics, Philadelphia, 2007), pp. 1099–1108.
[6] R. Portugal, *Quantum Walks and Search Algorithms* (Springer, Berlin, 2013).
[7] G. D. Paparo, M. Müller, F. Comellas, and M. A. Martin-Delgado, Sci. Rep. **3**, 2773 (2013).
[8] G. H. Weiss, *Aspects and Applications of the Random Walk* (North-Holland, Amsterdam, 1994).
[9] S. Redner, *A Guide to First-Passage Processes* (Cambridge University Press, Cambridge, 2001).
[10] C. Moore and S. Mertens, *The Nature of Computation* (Oxford University Press, Oxford, 2011).
[11] H. B. Perets, Y. Lahini, F. Pozzi, M. Sorel, R. Morandotti, and Y. Silberberg, Phys. Rev. Lett. **100**, 170506 (2008).
[12] L. Martin, G. D. Giuseppe, A. Perez-Leija, R. Keil, F. Dreisow, M. Heinrich, S. Nolte, A. Szameit, A. F. Abouraddy, D. N. Christodoulides, and B. E. A. Saleh, Opt. Express **19**, 13636 (2011).
[13] L. Sansoni, F. Sciarrino, G. Vallone, P. Mataloni, A. Crespi, R. Ramponi, and R. Osellame, Phys. Rev. Lett. **108**, 010502 (2012).
[14] A. Crespi, R. Osellame, R. Ramponi, V. Giovannetti, R. Fazio, L. Sansoni, F. D. Nicola, F. Sciarrino, and P. Mataloni, Nat. Photonics **7**, 322 (2013).
[15] C. Weitenberg, M. Endres, J. F. Sherson, M. Cheneau, P. Schauss, T. Fukuhara, I. Bloch, and S. Kuhr, Nature (London) **471**, 319 (2011).
[16] H. A. Carteret, M. E. H. Ismail, and B. Richmond, J. Phys. A **36**, 8775 (2003).
[17] T. D. Mackay, S. D. Bartlett, L. T. Stephenson, and B. C. Sanders, J. Phys. A **35**, 2745 (2002).
[18] A. C. Oliveira, R. Portugal, and R. Donangelo, Phys. Rev. A **74**, 012312 (2006).
[19] N. Inui and N. Konno, Phys. A (Amsterdam, Neth.) **353**, 133 (2005).
[20] N. Inui, N. Konno, and E. Segawa, Phys. Rev. E **72**, 056112 (2005).
[21] S. Falkner and S. Boettcher, Phys. Rev. A **90**, 012307 (2014).
[22] Y. Shikano and H. Katsura, Phys. Rev. E **82**, 031122 (2010).
[23] K. G. Wilson, Phys. Rev. B **4**, 3174 (1971).
[24] N. Goldenfeld, *Lectures on Phase Transitions and the Renormalization Group* (Addison-Wesley, Reading, MA, 1992).
[25] R. K. Pathria, *Statistical Mechanics*, 2nd ed. (Butterworth-Heinemann, Oxford, England, 1996).
[26] S. Boettcher, S. Falkner, and R. Portugal, J. Phys. Conf. Ser. **473**, 012018 (2013).
[27] S. Weber, J. Klafter, and A. Blumen, Phys. Rev. E **82**, 051129 (2010).
[28] D. A. Meyer, J. Stat. Phys. **85**, 551 (1996).
[29] R. Portugal, S. Boettcher, and S. Falkner, arXiv:1408.5166.
[30] A. Patel, K. S. Raghunathan, and P. Rungta, Phys. Rev. A **71**, 032347 (2005).
[31] M. Falk, arXiv:1303.4127.
[32] A. Ambainis, R. Portugal, and N. Nahimov, arXiv:1312.0172.
[33] S. Boettcher, B. Goncalves, and J. Azaret, J. Phys. A **41**, 335003 (2008).
[34] From the exact solution one finds that in this case the FP value m^* depends on the initial values for the RG flow, $1 - m^* = |a_0 - b_0|_{z=1}$, which cannot be obtained from the asymptotic analysis.
[35] A. Ambainis, E. Bach, A. Nayak, A. Vishwanath, and J. Watrous, in *Proceedings of the 33rd Annual ACM Symposium on Theory of Computing (STOC 2001)* (Association for Computing Machinery, New York, 2001), pp. 37–49.
[36] Nonzero values for χ, ϑ in Eq. (6) merely rotate this picture around the unit circle, i.e., affect a trivial shift in θ.
[37] P. C. S. Lara, R. Portugal, and S. Boettcher, Int. J. Quantum Inf. **11**, 1350069 (2013).